Micro-Raman Spectroscopy, a Powerful Technique Allowing Sure Identification and Complete Characterization of Asbestiform Minerals

Caterina Rinaudo *[ID] **and Alessandro Croce** *[ID]

Department of Science and Technological Innovation, University of Eastern Piedmont, Viale T. Michel 11, 15121 Alessandria, Italy
* Correspondence: caterina.rinaudo@uniupo.it (C.R.); alessandro.croce@uniupo.it (A.C.)

check for updates

Featured Application: Featured Application: Micro-Raman spectroscopy has been proved to be a quick technique for the study of minerals showing asbestiform morphology, in particular for identification of those ascribing to the phases defined by Law "asbestos". Moreover, information about the crystal surface—free or occupied by crystalline or amorphous particles—can be at the same time obtained, being this last feature important for the interaction of the fibers with the biological medium.

Abstract: Micro-Raman spectroscopy has been applied to fibrous minerals regulated as "asbestos"—anthophyllite, actinolite, amosite, crocidolite, tremolite, and chrysotile—responsible of severe diseases affecting mainly, but not only, the respiratory system. The technique proved to be powerful in the identification of the mineral phase and in the recognition of particles of carbonaceous materials (CMs) lying on the "asbestos" fibers surface. Also, erionite, a zeolite mineral, from different outcrops has been analyzed. To erionite has been ascribed the peak of mesothelioma noticed in Cappadocia (Turkey) during the 1970s. On the fibers, micro-Raman spectroscopy allowed to recognize many grains, micrometric in size, of iron oxy-hydroxides or potassium iron sulphate, in erionite from Oregon, or particles of CMs, in erionite from North Dakota, lying on the crystal surface. Raman spectroscopy appears therefore to be the technique allowing, without preparation of the sample, a complete characterization of the minerals and of the associated phases.

1. Introduction

Identification and characterization of the minerals constituting rocks, soils or dispersed in different matrixes has been at all times object of study for researchers working in the earth sciences. Mineralogists in particular applied optical microscopy (OM), scanning electron microscopy coupled with electron dispersive spectroscopy (SEM/EDS), X-ray powder diffraction (XRPD), transmission electron microscopy (TEM), etc., to obtain a complete characterization of the mineral phases. The normally used techniques often require preparation of the sample before analysis. Considering that the samples are often constituted by different crystalline phases, in variable amounts, which can be sometimes mixed with amorphous phases, it is obvious that the preparation of the samples for analysis may induce changes, loss of important information, and difficulties in the identification of phases in very low amounts. Micro-Raman spectroscopy, where an OM is coupled with the spectroscope, allows overcoming these inconveniences, mainly when OM is equipped with crossed nicols. In fact, the

technique can be applied directly on the samples, in a non-invasive way, and directing the laser beam in areas selected by the OM and characterized by optical peculiarities, heterogeneity in the sample can be easily highlighted. Moreover, Raman spectroscopy, supplying information on the vibrational modes of the chemical bonds, allows studying also materials in amorphous, gaseous, or liquid states.

Our research group operates in Alessandria, where the minerals regulated as "asbestos" have been, and are up till now, a serious problem consequent to the presence of an Eternit factory in Casale Monferrato, Alessandria (Italy), producing large quantities of asbestos-cement since the beginning of the last century until 1985 [1,2]. The asbestos are fibrous minerals with a high impact on the human health. In fact, to the inhalation of the asbestos fibers has been ascribed the development of severe respiratory diseases, in particular mesothelioma, asbestosis, and pulmonary carcinoma [3,4]. Other malignancies affecting extra-respiratory systems have been recognized as related to inhaled/ingested asbestos fibers. In particular, IARC recognized that the larynx and ovary tumors can be related to asbestos exposure [5] and various researchers are developing studies to verify the relationships between gastrointestinal cancers (GI) and asbestos [6–10].

We have been therefore interested in the identification of a technique able to identify surely fibers of asbestos, even when they are present in very low amounts. On the mineralogical point of view, the minerals regulated as "asbestos" [5,11,12] are:

- actinolite, theoretical chemical formula $Ca_2(Mg, Fe^{2+})_5[Si_8O_{22}](OH)_2$;
- amosite, theoretical chemical formula $(Fe^{2+}, Mg)_7[Si_8O_{22}](OH)_2$;
- anthophyllite, theoretical chemical formula $(Mg, Fe^{2+})_7[Si_8O_{22}](OH)_2$;
- crocidolite, theoretical chemical formula $Na_2Fe^{2+}_3Fe^{3+}_2[Si_8O_{22}](OH)_2$;
- tremolite, theoretical chemical formula $Ca_2Mg_5[Si_8O_{22}](OH)_2$,

when they exhibit fibrous habit. All these phases belong to amphibole group of silicates, where double chains of $[SiO_4]$ tetrahedra are each other linked by Na, Ca, Mg, Fe^{2+}, or Fe^{3+} cations, Figure 1a [12,13]. Being phases growing in a natural system, then with complex chemical composition of the mother solutions, very often homo- and etero-valent diadochy in the different crystallographic sites may occur. The real chemical formula therefore can differ from the theoretical one. As an example, in tremolite iron is not foreseen but substitutions of Mg by Fe^{2+} in the octahedral sites can be frequently observed.
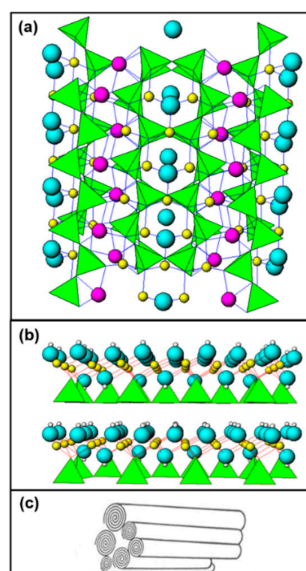

Figure 1. (**a**) Crystal structure of amphibole minerals: in green the $[SiO_4]$ tetrahedra, in blue the $(OH)^-$ groups, in yellow and in violet the Na, Ca, Mg, Fe^{2+}, or Fe^{3+} cations; (**b**) Crystal structure of serpentine minerals: in green the $[SiO_4]$ tetrahedra (T layers), in yellow the octahedral Mg cations (O layer), and in blue and white the OH^- groups; (**c**) In chrysotile T and O layers roll up around a hole forming long fibers.

The last mineral regulated as "asbestos" is:

- chrysotile, theoretical chemical formula $Mg_3Si_2O_5(OH)_4$.

This is a serpentine mineral [14], whose crystal structure is constituted by tetrahedra $[SiO_4]$ layers (T layer) and octahedra $(Mg\ O, OH)_6$ layers (O layer), where Mg^{2+} are linked to the $[SiO_4]$ tetrahedra and to OH^- ions, Figure 1b. Chrysotile exhibits a fibrous habit consequent to the rolling up of the T and the O layers around a hole, Figure 1c [15].

In this work, we describe the application of micro-Raman spectroscopy to fibers of the different "asbestos", proving its reliability not only in the identification of the minerals, but also of other phases lying on the fiber surfaces. In fact, the spectral range 4000–100 cm^{-1} has been recorded and presence on the fiber surfaces of particles, not necessarily crystalline, could be demonstrated.

The reasons of the carcinogenic effects of the "asbestos" has been extensively studied by different authors [4,16–18] and the dose of the inhaled fibers but also their morphology and the iron in the chemical formula have been described as factors determining their harmfulness [19,20]. As described before, growing these compounds in natural environment, iron can be present also in phases theoretically iron free. In vitro studies proved that, among "asbestos", the phases richest in iron, crocidolite and amosite, showed higher carcinogenic effects [21]. In addition to "asbestos", other minerals exhibiting fibrous habit have been proved to be responsible of asbestos-related diseases. Among all, erionite, a zeolite mineral showing an average chemical formula $K_2(Na, Ca_{0.5})_8[Al_{10}Si_{26}O_{72}]\cdot30H_2O$ has been considered responsible of the peak of mesothelioma, detected in Cappadocia (Turkey) during the 1970s [22–24]. On this, mineral iron is not a main chemical component, but erionite has been defined by the International Agency for Research on Cancer (IARC) more carcinogenic than asbestos [25].

Micro-Raman spectroscopy has therefore been applied also to samples of erionite from different localities (Oregon and North Dakota- USA- and Karlik- Cappadocia).

2. Materials and Methods

All the samples were analyzed under a HORIBA JobinYvon HR800 LabRam μ-spectrometer (HORIBA Jobin Yvon, Paris, France), coupled with an Olympus BX41 microscope (Olympus, Tokyo, Japan). The used excitation source was a HeNe laser, 20 mW, working at 632.8 nm, and the detector was an air-cooled charge-coupled device (CCD). Spectrometer calibration was obtained checking position and intensity of the Si band at 520.65 ± 0.05 cm^{-1}. The analyses were performed with a timing of at least 2 cycles of 200 s, after introduction of D06 filter to prevent sample modification, and a confocal hole set at 200 μm. ORIGIN software v 6.0 was applied on the recorded spectra. The asymmetric bands were treated with OPUS software to obtain fitting process after 13 points FFT smoothing of the spectrum and selecting a Lorentzian function and minimum number of component bands to obtain reproducible results with the minimal residual error.

SEM analyses were carried out using an environmental SEM (E-SEM; model Quanta 200, FEI Company, Hillsboro, OR, USA), with a pressure of 90 Pa, an accelerating voltage of 20 kV, and a working distance of 10 mm. Observation of phases with different chemical composition on the fiber surface was easy thanks to the back-scattered electron detector (BSED) and the generated white-black contrasts, not so evident using secondary electrons (SE).

For the six minerals, regulated as "asbestos", the studied samples were:

a. amosite from South Africa;
b. UICC crocidolite reference sample from South Africa;
c. tremolite from Brachiello (Val d'Ala, Piedmont region);
d. anthophyllite from Bresimo mine (Trentino Alto Adige, Italy);
e. actinolite certified by IOM (Institute of Occupational Medicine);
f. UICC chrysotile reference sample "B" Canadian (NB #4173-111-1) from Quebec, Canada.

The a.–d. minerals have been previously characterized with the traditionally used techniques (XRPD, SEM/EDS, TEM/EDS, and Analytical Electron Microscopy- AEM) and stated in Rinaudo et al.

2004 [26], whereas for chrysotile, the crystal structure and chemistry was described in Pollastri et al. 2016 [27].

Oregon and Cappadocia erionite chemicals were determined by Dogan et al. 2006 [28], while North Dakota chemical composition was compared with Turkish samples in Carbone et al. 2011 [22].

For each studied mineral phase, different spectra from various bundles of fibers were recorded in the spectral range 4000–100 cm^{-1}. When particles were observed on the fiber surface by means of the OM annexed to spectrometer, micro-Raman spectra were recorded directing the laser beam onto the grains.

3. Results and Discussion

Considering the "asbestos" minerals, more or less numerous particles, mostly rounded and micrometric in size, were observed on their fiber surface under OM, Figure 2. The phenomenon was particularly evident on amosite, Figure 2a, where the fibers were practically recovered both by fine fibrils and by small particles. Also crocidolite, Figure 2b, and chrysotile, Figure 2f, exhibited many dark particles on their surface, but also areas free from these foreign phases could be observed. On tremolite, anthophyllite and actinolite, the presence of round grains was less frequently noticed, Figure 2c–e.
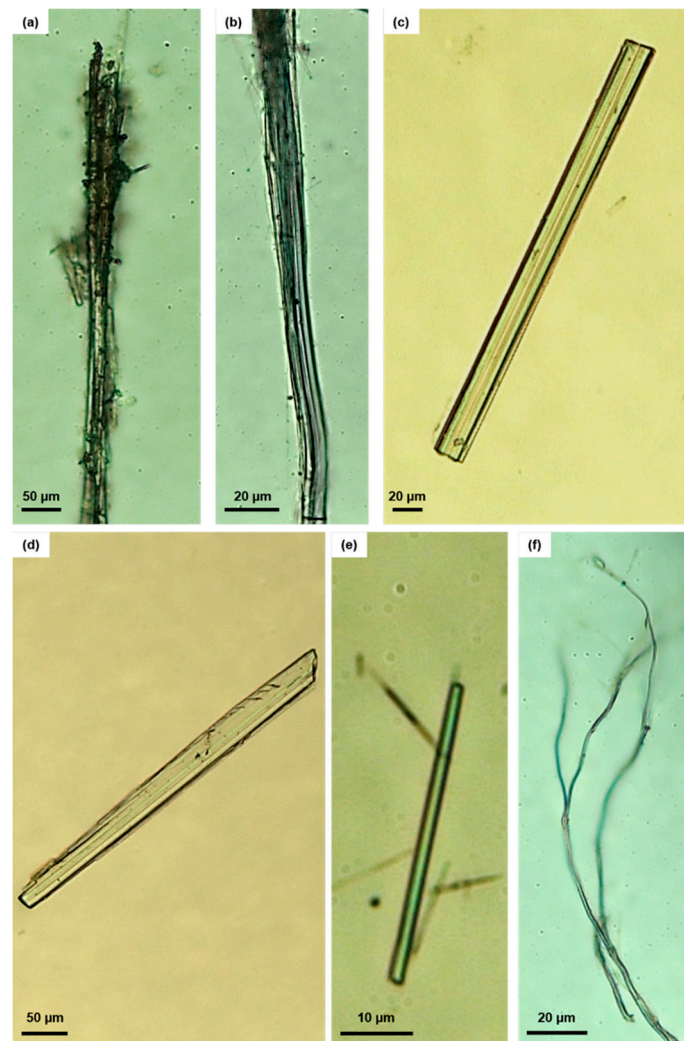

Figure 2. Optical Microscopy images of the six regulated asbestos minerals: (**a**) amosite; (**b**) crocidolite; (**c**) tremolite; (**d**) anthophyllite; (**e**) actinolite; (**f**) chrysotile.

The data from micro-Raman spectroscopy can be analyzed for the spectral region where lie the vibrational modes ascribed to the three-dimensional lattice of the mineral phases, 1200–100 cm^{-1}, and for the spectral range, 4000–1200 cm^{-1}, where lie the non-reticular vibrational modes. As it concerns the first spectral region, the results are shown in Figure 3. The Raman spectra appeared very rich in bands, especially in amphiboles, as a consequence of the different chemical bonds in the crystal structure (Si-O$_b$-Si, Si-O, bonds between various cations and tetrahedral oxygens or OH$^-$ groups ...), therefore the attribution of each band to a single vibrational mode is very hard and in any case beyond the aim of this work. A discussion about the vibrational modes produced by the stretching modes, both symmetric (ν_s) and antisymmetric (ν_{as}), of the different Si-O linkages has been proposed in Rinaudo et al. 2004 [26], and recently determination of the chemical formulae of various amphiboles by Raman spectroscopy has been suggested by Waeselmann et al. 2019 [29]. On the contrary, the Raman spectrum from chrysotile appeared poorer in bands, consequence of a crystal structure formed by only two types of polyhedra—SiO$_4$ and Mg(O, OH)$_6$. For the serpentine minerals, an attribution of the detected Raman bands to the different vibrational modes has been described in Rinaudo et al. 2003 [30].
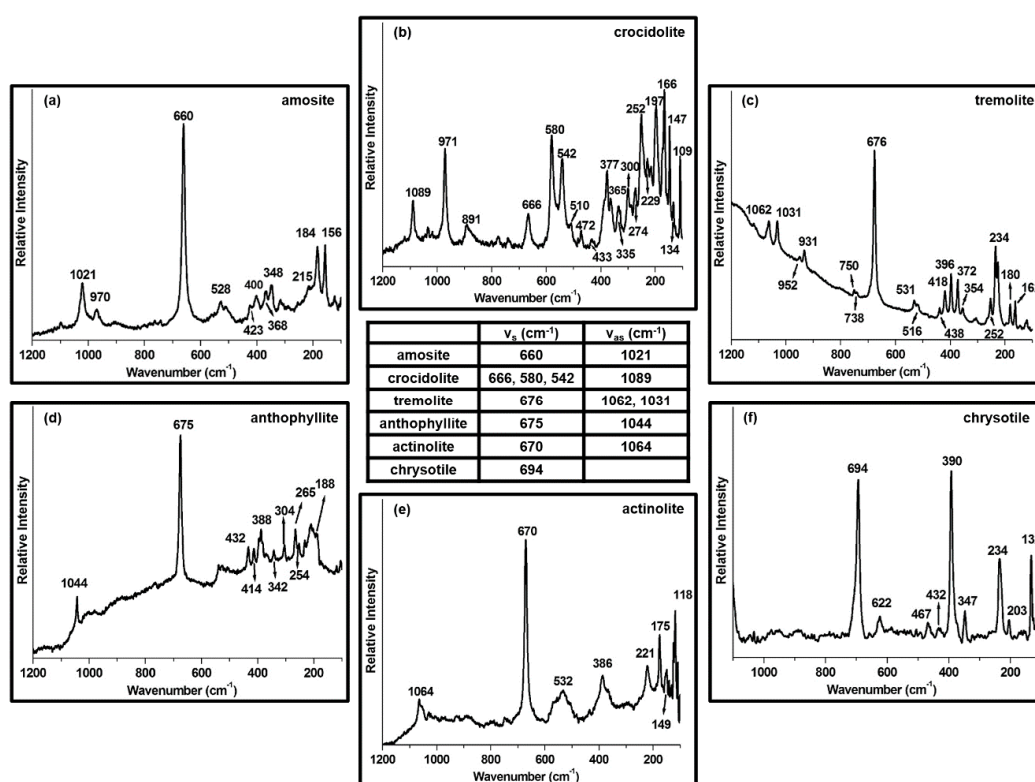

	ν_s (cm^{-1})	ν_{as} (cm^{-1})
amosite	660	1021
crocidolite	666, 580, 542	1089
tremolite	676	1062, 1031
anthophyllite	675	1044
actinolite	670	1064
chrysotile	694	

Figure 3. Spectra obtained on the six regulated asbestos minerals in the spectral range 1200–100 cm^{-1}: (**a**) amosite; (**b**) crocidolite; (**c**) tremolite; (**d**) anthophyllite; (**e**) actinolite; (**f**) chrysotile. Considering the ν_s and ν_{as} modes of the Si-O$_b$-Si bonds, a sure identification of the mineral phase can be obtained.

Being interested in the identification of the mineral phase, it can be achieved considering the region where lie the symmetric stretching modes (ν_s), 700–600 cm^{-1}, and antisymmetric stretching modes (ν_{as}), 1100–1000 cm^{-1}, of the Si-O$_b$-Si linkages, Figure 3. In fact, the difference in wavenumbers where lie the ν_s modes is higher than the instrumental error, 2 cm^{-1}. A particular situation involves tremolite and anthophyllite, where the ν_s modes vibrate very close. In this case, considering also the wavenumbers of the ν_{as} stretching modes (1044 cm^{-1} in anthophyllite and 1062 and 1031 cm^{-1} in tremolite), a sure identification can be achieved. As it concerns chrysotile, the ν_s modes vibrate at higher wavenumber, about 694 cm^{-1}, with respect to all the amphibole asbestos phases. Concerning the ν_{as} stretching modes, lying at 1105 cm^{-1}, it is often undetectable for the presence of intense bands

produced by carbonaceous materials (CMs) lying on the crystal surface [31], Figure 3f, as will be after discussed.

In the spectral region 4000–1200 cm^{-1} on amosite, appearing under OM practically recovered by round dark particles, Figure 2a, bands ascribing to carbonaceous materials have been almost always detected, Figure 4a. In fact, bands at 1332, 1582, and 2663 cm^{-1} have been observed and they can be ascribed respectively to D (diamond like), G (graphite like) and G′ (second order Raman scattering) vibrations of CMs [31].

Also on crocidolite, showing often under OM dark particles on the crystal surface, Figure 2b, bands ascribed to CMs were identified when the laser beam was directed onto the grains, Figure 4b. On the spectra, the bands at 1333, 1600, 2660, and 2914 cm^{-1} can be ascribed respectively to D, G, G′, and C-H vibrations. The fact that on crocidolite the band at 1333 cm^{-1} showed higher intensity with respect to the band near 1600 cm^{-1}, which appears large, proves a higher disorder in the CM particles lying on the crystal structure. On the other hand, applying fitting program to the 1600 cm^{-1} band, two underlying bands at 1591 (G vibrations) and 1621 (D′ vibrations) cm^{-1} were identified (box in Figure 4b), confirming carbonaceous grains rich in defects.

On the other amphibole phases, especially on actinolite and anthophyllite, bands ascribed to CMs were very rarely observed, confirming the data from OM observations, Figure 2c–e. On tremolite, at wavenumbers higher than 1200 cm^{-1}, an intense and large hump produced by fluorescence effects was always detected. This fact avoided detection of Raman bands in this spectral range.

On chrysotile, in the 4000–1100 cm^{-1} spectral range, different bands ascribing to carbonaceous materials were detected, Figure 4f. In particular the band at 1118 cm^{-1} may be ascribed to symmetric stretching of C-O-C bonds, the band at 1273 cm^{-1} to disordered C-H, the band at 1340 cm^{-1} produced by D vibrations, the band at 1613 cm^{-1} by G + D′ vibrations, and the band at 1690 cm^{-1} due to C=O bonds [31,32].
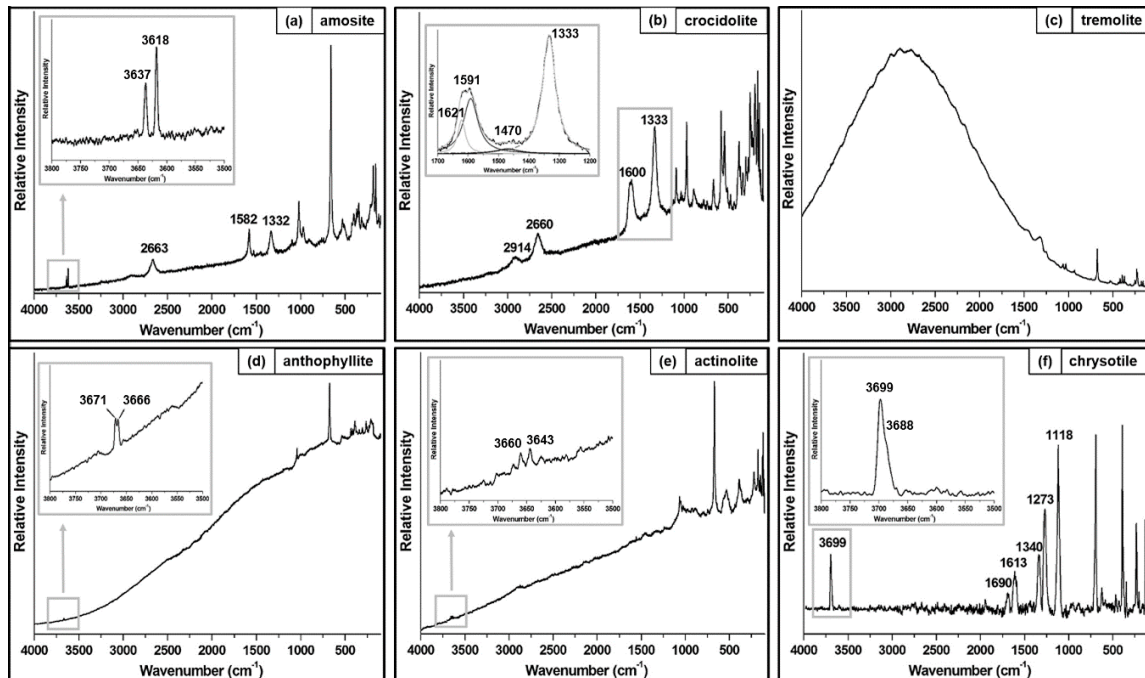

Figure 4. Raman spectra of the 4000–100 cm^{-1} range obtained on the six regulated asbestos minerals: (**a**) amosite; (**b**) crocidolite; (**c**) tremolite; (**d**) anthophyllite; (**e**) actinolite; (**f**) chrysotile.

With the laser wavelength used, 632.8 nm, the OH$^-$ vibrations were detected only on amosite, bands at 3618 and 3637 cm^{-1}, anthophyllite at 3666 and 3671 cm^{-1}, actinolite at 3643 and 3660 cm^{-1}, and chrysotile, bands at 3688 and 3699 cm^{-1}.

The position of the obtained Raman bands are summarized in Tables 1 and 2.

Table 1. Raman bands observed on the mineral phases defined "asbestos" by the Law.

Mineral Phase	Amosite This Work	Amosite Rinaudo et al. 2004 [26]	Crocidolite This Work	Crocidolite Rinaudo et al. 2004 [26]	Tremolite This Work	Tremolite Rinaudo et al. 2004 [26]
Mineral Raman Bands (cm^{-1})	156	155	109		162	162
	184	182	134		180	180
	215	216	147			225
		252	166	162	234	234
		289	197	195	252	254
		307		211		290
	348	348	229			306
	368	368	252	246		335
	400	400	274	272		348
	423	423	300	300	354	355
		507	335	331	372	373
	528	528	365	360	396	396
	660	659	377	374	418	418
		904	433	428	438	438
	970	968	472	470	516	516
	1021	1020	510	506	531	531
		1093	542	537	676	676
			580	577	738	740
			666	664	750	751
				733	931	932
				771	952	950
			891	889	1031	1031
			971	967	1062	1062
				1030		
			1089	1082		
CM Raman Bands (cm^{-1})	1332		1333		-	
			1470		-	
	1582	n.a. *	1591	n.a.	-	n.a.
			1621		-	
	2663		2660		-	
			2914		-	
OH$^-$ Raman Bands (cm^{-1})	3618	n.a.	-	n.a.	-	n.a.
	3637		-		-	

* n.a.: not available.

Table 2. Raman bands observed on the mineral phases defined "asbestos" by the Law.

Mineral Phase	Anthophyllite This Work	Anthophyllite Rinaudo et al. 2004 [26]	Actinolite This Work	Chrysotile This Work	Chrysotile Rinaudo et al. 2003 [30]
Mineral Raman Bands (cm^{-1})	188	188	118	132	
		222	149	203	
	254	254	175	234	231
	265	265	221	347	345
	304	304	386	390	389
	342	342	532	432	
		364	670	467	
	388	387	1064	622	620
	414	410		694	692
	432	433			1105
		503			
		539			
	675	674			
		699			
		928			
	1044	1044			
CM Raman Bands (cm^{-1})	-		-	1118	
	-		-	1273	
	-		-	1340	
	-	n.a. *	-	1613	n.a.
	-		-	1690	
	-		-		
	-				
OH$^-$ Raman Bands (cm^{-1})	3666	n.a.	3643	3688	n.a.
	3671		3660	3699	

* n.a.: not available.

Considering now the erionite samples, the spectral range where lie the lattice vibrational modes appeared poorer in Raman bands. In fact, only an intense band at about 485 cm^{-1}, with an evident component at about 470 cm^{-1}, and weaker bands at about 570, 330–345, and 127–140 cm^{-1} characterized the Raman spectrum, Figure 5.
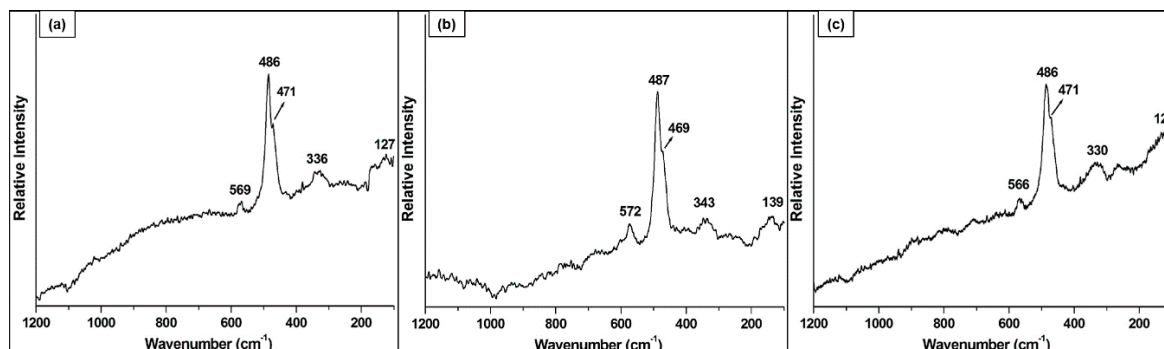

Figure 5. Raman spectra in the 1200–100 cm^{-1} range obtained on erionite from (**a**) Oregon, (**b**) Karlik, and (**c**) North Dakota.

Nevertheless, all the studied erionite fibers exhibited, under SEM, particles, sub-micrometric in size, lying on the crystal surface, Figure 6.
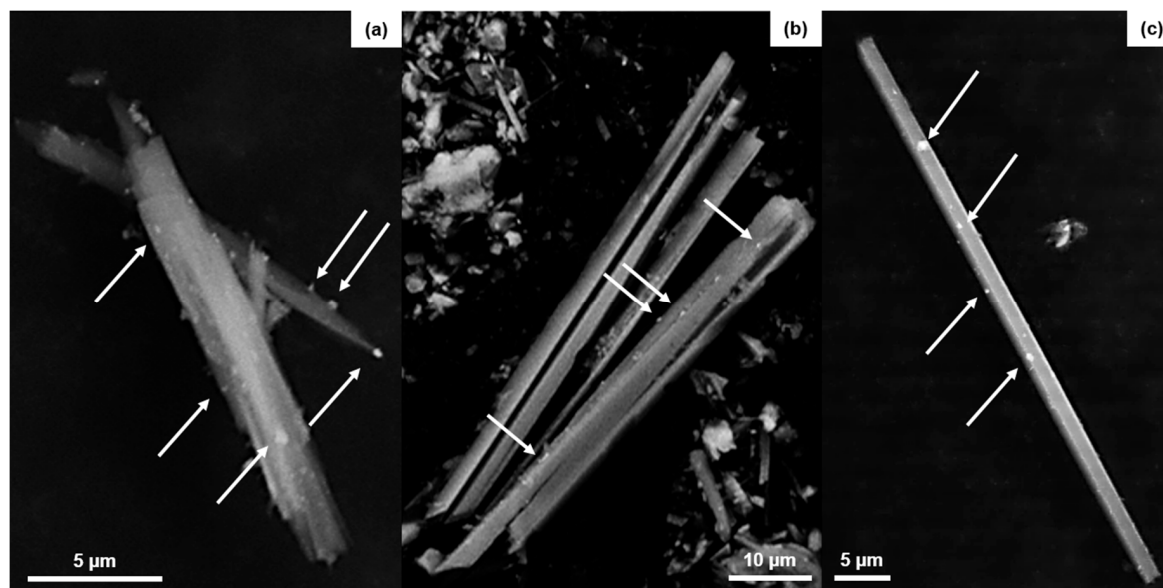

Figure 6. Backscattered scanning electron microscopy (SEM) images of erionite fibers from (**a**) Oregon, (**b**) Karlik, and (**c**) North Dakota. The arrows indicate particles lying on the crystal surfaces.

Directing the laser beam onto the observed grains, different results were obtained on erionite from the various outcrops. In particular on the erionite from Oregon, the Raman spectra recorded on the grains identified:

- Goethite, chemical formula FeO(OH), Raman spectra as that shown in Figure 7a. In this case the band at 395 cm^{-1} resulted, with respect to the value, 385 cm^{-1}, normally observed on this mineral, shifted of 10 cm^{-1} as consequence of a poor crystallinity of the grains [33,34];
- Hematite, chemical formula Fe$_2$O$_3$, spectra as that shown in Figure 7b [34,35];
- Jarosite, KFe$_3^{3+}$(SO$_4$)$_2$(OH)$_6$, an iron-potassium sulphate [35,36], Figure 7c. On the Raman spectrum recorded on the grains of jarosite, the presence of a band at 387 cm^{-1}, not ascribing to this mineral phase, indicated a contemporaneous crystallization of small amounts of goethite [34,35].

Therefore, the described results indicated many iron particles lying on the surface of the erionite fibers. Considering that iron is a co-factor in the fiber carcinogenicity [21] and that the IARC indicated this mineral phase more carcinogenic than asbestos [25], the role of the iron particles on the fiber surface may play a synergic role in the pathogenicity of this mineral.
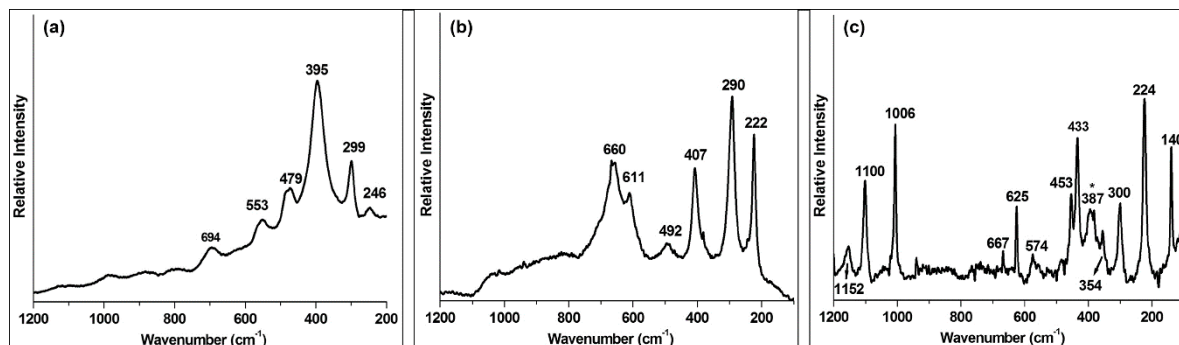

Figure 7. Raman spectra of the 1200–100 cm^{-1} range obtained on different iron rich particles on erionite: (**a**) goethite, (**b**) hematite, and (**c**) jarosite. The band indicated by * in (**c**) may be ascribed to goethite.

On the fibers from North Dakota, the Raman spectrum more frequently recorded is shown in Figure 6c. In this case, the Raman bands in the spectral region corresponding to lattice vibrations agree with the data obtained on erionite from Oregon and Karlik, but in the part of the spectrum 4000–1200 cm^{-1} bands ascribed to carbonaceous materials were almost always observed, Figure 8. On this mineral the D band lies at 1336 cm^{-1}, the G + D' band at 1604 cm^{-1}, the G' band at 2655 cm^{-1}, whereas the bands at 1450, 2878 and 2914 cm^{-1} can be ascribed to C-H bonds.

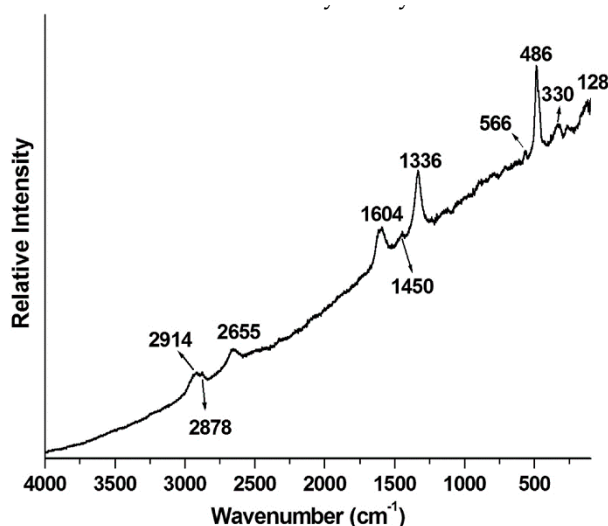Carbonaceous materials have been detected very rarely on erionite from Oregon and from Karlik.

Figure 8. Raman spectra obtained in the 4000–100 cm^{-1} range on a dark grain on the surface of North Dakota erionite fibers.

4. Conclusions

It is now universally accepted the noxious role of the asbestos on the human health. Asbestos fibers in the human body can be detected not only in the respiratory system, when inhaled [18,37,38], but also in other organs or tissues [39–43], attained by translocation or ingestion processes. Considering that recent studies demonstrated its presence in unexpected places, in paintings as an example [44], it is therefore very important to find a technique allowing an easy identification of the fibers in different matrixes.

From all the above described data, micro-Raman spectroscopy appears the good technique for identification of mineral phase associated with fibers or bundle of fibers. It is a technique allowing to record spectra directly on the samples and on materials in crystalline and amorphous state. On asbestos it allowed not only to identify the phase, but also to highlight carbonaceous materials lying on the crystal surface, never recognized with the traditionally used techniques. It is known that carbonaceous particles, when inhaled, may constitute a problem for the human health [45,46]. Being stuck on the asbestos fibers, especially on amosite, crocidolite, and chrysotile, the most commonly used in the industry in the past, they may contribute to increase the noxious effects of these asbestiform minerals.

Also on erionite, a mineral phase not regulated but recognized more carcinogenic than asbestos, micro-Raman spectroscopy allowed to recognize, mainly on Oregon erionite fibers [35], many particles of iron oxy-hydroxides or sulphates. The role of iron in the pathogenicity of the fibers has been demonstrated. On erionite fibers from North Dakota, dark grains lying on the crystal surface have been recognized as carbonaceous particles, as those detected on the "asbestos".

Although in this work micro-Raman spectroscopy has been applied on asbestiform phases, the technique contribution in an in-depth characterization of the minerals, of the mineral association, and generally of materials appears un-doubted. Moreover, the possibility of studies in a non-destructive way, maintaining unaltered the relationship among the different components of the analyzed samples, appears a very interesting peculiarity of the technique.

References

1. Martuzzi, M.; Comba, P.; De Santis, M.; Iavarone, I.; Di Paola, M.; Mastrantonio, M.; Pirastu, R. Asbestos-related lung cancer mortality in Piedmont, Italy. *Am. J. Ind. Med.* **1998**, *33*, 565–570. [CrossRef]

2. Magnani, C.; Dalmasso, P.; Biggeri, A.; Ivaldi, C.; Mirabelli, D.; Terracini, B. Increased risk of malignant mesothelioma of the pleura after residential or domestic exposure to asbestos: A case-control study in Casale Monferrato, Italy. *Environ. Health Perspect.* **2001**, *109*, 915–919. [CrossRef] [PubMed]

3. Bartrip, P.W.J. History of asbestos related disease. *Postgrad. Med. J.* **2004**, *80*, 72–76. [CrossRef] [PubMed]

4. Carbone, M.; Ly, B.H.; Dodson, R.F.; Pagano, I.; Morris, P.T.; Dogan, U.A.; Gazdar, A.F.; Pass, H.I.; Yang, H. Malignant mesothelioma: Facts, myths, and hypotheses. *J. Cell. Physiol.* **2012**, *227*, 44–58. [CrossRef]

5. International Agency for Research on Cancer (IARC). Asbestos (chrysotile, amosite, crocidolite, tremolite, actinolite, and anthophyllite). In *IARC Monographs on the Evaluation of Carcinogenic Risks to Humans*; IARC: Lyon, France, 2012; Volume 100, pp. 219–309.

6. Brandi, G.; Di Girolamo, S.; Belpoggi, F.; Grazi, G.; Ercolani, G.; Biasco, G. Asbestos exposure in patients affected by bile duct tumours. *Eur. J. Oncol.* **2008**, *13*, 171–179.

7. Brandi, G.; Di Girolamo, S.; Farioli, A.; de Rosa, F.; Curti, S.; Pinna, A.D.; Ercolani, G.; Violante, F.S.; Biasco, G.; Mattioli, S. Asbestos: A hidden player behind the cholangiocarcinoma increase? Findings from a case–control analysis. *Cancer Causes Control* **2013**, *24*, 911–918. [CrossRef]

8. Di Ciaula, A. Asbestos ingestion and gastrointestinal cancer: A possible underestimated hazard. *Expert Rev. Gastroenterol. Hepatol.* **2017**, *11*, 419–425. [CrossRef]

9. Di Ciaula, A.; Gennaro, V. Possible health risks from asbestos in drinking water. *Epidemiol. Prev.* **2016**, *40*, 472–475.

10. Farioli, A.; Straif, K.; Brandi, G.; Curti, S.; Kjaerheim, K.; Martinsen, J.I.; Sparen, P.; Tryggvadottir, L.; Weiderpass, E.; Biasco, G.; et al. Occupational exposure to asbestos and risk of cholangiocarcinoma:

A population-based case–control study in four Nordic countries. *Occup. Environ. Med.* **2018**, *75*, 191–198. [CrossRef]

11. Italian Government. Legislative Decree No. 277 of 15 August 1991, Implementing EU Directives No. 80/1107/EEC, No. 82/605/EEC, No. 83/477/EEC, No. 86/188/EEC, and No. 88/642/EEC, on the Protection of Workers from the Risks Related to Exposure to Chemical, Physical and Biological Agents at Work. Gazzetta Ufficiale Supplemento Ordinario No. 200. 27 August 1991. Available online: https://www.gazzettaufficiale.it/atto/serie_generale/caricaDettaglioAtto/originario?atto.dataPubblicazioneGazzetta=1991-08-27&atto.codiceRedazionale=091G0311&elenco30giorni=false (accessed on 4 July 2019).

12. Leake, B.E.; Woolley, A.R.; Arps, C.E.S.; Birch, W.D.; Gilbert, M.C.; Grice, J.D.; Hawthorne, F.C.; Kato, A.; Kisch, H.J.; Krivovichev, V.G.; et al. Nomenclature of amphiboles: Report of the Subcommittee on amphiboles of the International Mineralogical Association, Commission on New Minerals and Mineral Names. *Can. Mineral.* **1997**, *35*, 219–246.

13. Hawthorne, F.C.; Oberti, R.; Harlow, G.E.; Maresch, W.V.; Martin, R.F.; Schumacher, J.C.; Welch, M.D. Nomenclature of the amphibole supergroup. *Am. Mineral.* **2012**, *97*, 2031–2048. [CrossRef]

14. Whittaker, E.J.W.; Zussman, J. The characterization of serpentine minerals by X-ray diffraction. *Mineral. Mag.* **1956**, *233*, 107–126. [CrossRef]

15. Putnis, A. The crystal structure of minerals II—Silicates. In *Introduction to Mineral Sciences*; Cambridge University Press: Cambridge, UK, 1992; pp. 141–184.

16. Aust, A.E.; Cook, P.M.; Dodson, R.F. Morphological and chemical mechanisms of elongated mineral particle toxicities. *J. Toxicol. Environ. Health Part B* **2011**, *14*, 40–75. [CrossRef] [PubMed]

17. Fubini, B.; Mollo, L. Role of iron in the reactivity of mineral fibers. *Toxicol. Lett.* **1995**, *82–83*, 951–960. [CrossRef]

18. Yao, S.; Della Ventura, G.; Petibois, C. Analytical characterization of cell-asbestos fiber interactions in lung pathogenesis. *Anal. Bioanal. Chem.* **2010**, *397*, 2079–2089. [CrossRef]

19. Stanton, M.F.; Layard, M.; Tegeris, A.; Miller, E.; May, M.; Morgan, E.; Smith, A. Relation of particle dimension to carcinogenicity in amphibole asbestoses and other fibrous minerals. *J. Natl. Cancer Inst.* **1981**, *67*, 965–975.

20. Prandi, L.; Tomatis, M.; Penazzi, N.; Fubini, B. Iron cycling mechanisms and related modifications at the asbestos surface. *Ann. Occup. Hyg.* **2002**, *46* (Suppl. I), 140–143.

21. Lund, L.G.; Aust, A.E. Iron mobilization from crocidolite asbestos greatly enhances crocidolite-dependent formation of DNA single-strand breaks in φ X174 RFI DNA. *Carcinogenesis* **1992**, *13*, 637–642. [CrossRef]

22. Carbone, M.; Baris, Y.I.; Bertino, P.; Brass, B.; Comertpay, S.; Dogan, A.U.; Gaudino, G.; Jube, S.; Kanodia, S.; Partridge, C.R.; et al. Erionite exposure in North Dakota and Turkish villages with mesothelioma. *Proc. Natl. Acad. Sci. USA* **2011**, *108*, 13618–13623. [CrossRef]

23. Dogan, A.U.; Dogan, M.; Hoskins, J.A. Erionite and its Health Effects. In *Encylopedia of Environmental Health*; Nriagu, J.O., Ed.; Elsevier: Burlington, MA, USA, 2011; Volume 2, pp. 590–593.

24. Emri, S.A. The Cappadocia mesothelioma epidemic: Its influence in Turkey and abroad. *Ann. Transl. Med.* **2017**, *5*, 239. [CrossRef]

25. International Agency for Research on Cancer (IARC). Erionite. In *IARC Monographs on the Evaluation of Carcinogenic Risks to Humans*; IARC: Lyon, France, 2012; Volume 100, pp. 311–316.

26. Rinaudo, C.; Belluso, E.; Gastaldi, D. Assessment of the use of Raman spectroscopy for the determination of amphibole asbestos. *Mineral. Mag.* **2004**, *68*, 455–465. [CrossRef]

27. Pollastri, S.; Perchiazzi, N.; Lezzerini, M.; Plaisier, J.R.; Cavallo, A.; Dalconi, M.C.; Bursi Gandolfi, N.; Gualtieri, A.F. The crystal structure of mineral fibres 1. Chrysotile. *Period. Mineral.* **2016**, *85*, 249–259.

28. Dogan, A.U.; Baris, Y.I.; Dogan, M.; Emri, S.; Steele, I.; Elmishad, A.G.; Carbone, M. Genetic predisposition to fiber carcinogenesis causes a mesothelioma epidemic in Turkey. *Cancer Res.* **2006**, *66*, 5063–5068. [CrossRef] [PubMed]

29. Waeselmann, N.; Schlüter, J.; Malcherek, T.; Della Ventura, G.; Oberti, R.; Mihailova, B. Nondestructive determination of the amphibole crystal-chemical formulae by Raman spectroscopy: One step closer. *J. Raman Spectrosc.* **2019**. [CrossRef]

30. Rinaudo, C.; Gastaldi, D.; Belluso, E. Characterization of chrysotile, antigorite and lizardite by FT-Raman spectroscopy. *Can. Mineral.* **2003**, *41*, 883–890. [CrossRef]

31. Croce, A.; Arrais, A.; Rinaudo, C. Raman micro-spectroscopy identifies carbonaceous particles lying on the surface of crocidolite, amosite, and chrysotile fibers. *Minerals* **2018**, *8*, 249. [CrossRef]

32. Bonoldi, L.; Frigerio, F.; Di Paolo, L.; Savoini, A.; Barbieri, D.; Grigo, D. Organic matter maturity profile of a well case study by combination of Raman spectroscopy and principal component analysis−partial least squares regression (PCA−PLS) chemometric methods. *Energy Fuels* **2018**, *32*, 8955–8965. [CrossRef]

33. Bourchand, M.; Smith, D.C. Catalogue of 45 reference Raman spectra of minerals concerning research in art history or archaeology, especially on corroded metals and coloured glass. *Spectrochim. Acta A Mol. Biomol. Spectrosc.* **2003**, *59*, 2247–2266.

34. Hanesch, M. Raman spectroscopy of iron oxides and (oxy)hydroxides at low laser power and possible applications in environmental magnetic studies. *Geophys. J. Int.* **2009**, *177*, 941–948. [CrossRef]

35. Croce, A.; Allegrina, M.; Rinaudo, C.; Gaudino, G.; Yang, H.; Carbone, M. Numerous iron-rich particles lie on the surface of erionite fibers from Rome (Oregon, USA) and Karlik (Cappadocia, Turkey). *Microsc. Microanal.* **2015**, *21*, 1341–1347. [CrossRef]

36. Sasaki, K.; Tanaike, O.; Konno, H. Distinction of jarosite-group compounds by Raman spectroscopy. *Can. Mineral.* **1998**, *36*, 1225–1235.

37. Rinaudo, C.; Allegrina, M.; Fornero, E.; Musa, M.; Croce, A.; Bellis, D. Micro-Raman spectroscopy and VP-SEM/EDS applied to the identification of mineral particles and fibres in histological sections. *J. Raman Spectrosc.* **2010**, *41*, 27–32. [CrossRef]

38. Rinaudo, C.; Croce, A.; Musa, M.; Fornero, E.; Allegrina, M.; Trivero, P.; Bellis, D.; Sferch, D.; Toffalorio, F.; Veronesi, G.; et al. Study of inorganic particles, fibers, and asbestos bodies by variable pressure scanning electron microscopy with annexed energy dispersive spectroscopy and micro-Raman spectroscopy in thin sections of lung and pleural plaque. *Appl. Spectrosc.* **2010**, *64*, 571–577. [CrossRef] [PubMed]

39. Croce, A.; Capella, S.; Belluso, E.; Grosso, F.; Mariani, N.; Libener, R.; Rinaudo, C. Asbestos fibre in gallbladder: A case study. *Micron* **2018**, *105*, 98–104. [CrossRef] [PubMed]

40. Ehrlich, A.A.; Gordon, R.E.; Dikman, S.H. Carcinoma of the colon in asbestos-exposed workers: Analysis of asbestos content in colon tissue. *Am. J. Ind. Med.* **1991**, *19*, 629–636. [CrossRef] [PubMed]

41. Grosso, F.; Croce, A.; Libener, R.; Mariani, N.; Pastormerlo, M.; Maconi, A.; Rinaudo, C. Asbestos fiber identification in liver from cholangiocarcinoma patients living in an asbestos polluted area: A preliminary study. *Tumori J.* **2019**. [CrossRef] [PubMed]

42. Grosso, F.; Croce, A.; Trincheri, N.F.; Mariani, N.; Libener, R.; Degiovanni, D.; Rinaudo, C. Asbestos fibres detected by scanning electron microscopy in the gallbladder of patients with malignant pleural mesothelioma (MPM). *J. Microsc.* **2017**, *266*, 48–54. [CrossRef] [PubMed]

43. Grosso, F.; Randi, L.; Croce, A.; Mirabelli, D.; Libener, R.; Magnani, C.; Bellis, D.; Allegrina, M.; Bertolotti, M.; Degiovanni, D.; et al. Asbestos fibers in the gallbladder of patients affected by benign biliary tract diseases. *Eur. J. Gastroenterol. Hepatol.* **2015**, *27*, 660–664. [CrossRef]

44. Kakoulli, I.; Prikhodko, S.V.; King, A.; Fischer, C. Earliest evidence for asbestos composites linked to Byzantine wall paintings production. *J. Archaeol. Sci.* **2014**, *44*, 148–153. [CrossRef]

45. Donaldson, K.; Poland, C.A.; Murphy, F.A.; MacFarlane, M.; Chernova, T.; Schinwald, A. Pulmonary toxicity of carbon nanotubes and asbestos—Similarities and differences. *Adv. Drug Deliv. Rev.* **2013**, *65*, 2078–2086. [CrossRef]

46. International Agency for Research on Cancer (IARC). Carbon black, titanium dioxide, and talc. In *IARC Monographs on the Evaluation of Carcinogenic Risks to Humans*; IARC: Lyon, France, 2010; Volume 93, pp. 43–191.